# APPLICATION OF SATELLITE PRECIPITATION DATA TO MODEL THE EXTREME RAINFALL-INDUCED LANDSLIDE EVENT

THAPTHAI CHAITHONG
*Department of Geography, Faculty of Social Sciences, Kasetsart University, Bangkok, Thailand, thapthai.c@gmail.com*

DAISUKE KOMORI
*Department of Civil and Environmental Engineering, Graduate School of Engineering, Tohoku University, Sendai, Japan, daisuke.komori.e8@tohoku.ac.jp*

## ABSTRACT

Precipitation data are fundamental to generating a landslide hazard map or for back-calculating landslide events. The spatial variation characteristic of precipitation data plays a critical role in the spatial analysis of landslides. Traditionally, observation data from rain-gauge stations and spatial interpolation techniques such as IDW or Kriging are used to generate the spatial data of precipitation. This method can analyze landslide events, but it is limited by the number of rain-gauge stations in the study area and the conditions for the spatial interpolation methods. In recent years, satellite precipitation data have been developed and collected by numerous organizations such as Global Precipitation Measurement (GPM) and the Tropical Rainfall Measuring Mission (TRMM). Satellite precipitation data can provide good regional information about the distribution of rainfall, especially when compared to rain-gauge data. However, there are disadvantages to satellite precipitation data such as coarse resolution and questionable accuracy. The purpose of this study is to propose a conceptual framework for spatial analysis of extreme rainfall-induced landslides using satellite precipitation data from a case study of tropical storm Nanmadol (2017) in the city of Asakura, Fukuoka prefecture, Japan. The satellite precipitation data were calibrated and downscaled to obtain the final rainfall dataset. The rainfall-induced landslide model was developed based on a combination of the Green-Ampt infiltration model and the infinite slope model. According to our calculations, this conceptual framework using satellite precipitation data can identify landslide areas in the city of Asakura, Fukuoka prefecture, Japan.

*Keywords*: Satellite precipitation, extreme rainfall, landslide, typhoon, slope failure

## 1. INTRODUCTION

Landslides triggered by rainfall in Japan commonly occur during the Typhoon season. Numerous researchers have reported cases of typhoon-induced landslides (Kawamoto et al., 2000; Yokoyama et al., 2006; Sehara et al., 2006; Taniguchi, 2008; Murakami et al., 2008; Sakurai, 2014; Chaithong, et al., 2018; and Hazarika et al., 2020). Several factors influence landslide occurrences such as soil properties or topography, but the amount of rainfall is the most significant. Lim et al. (1996) monitored and analyzed residual hillslopes in Singapore. They found that matric suctions were reduced during and after rainfalls and the perched water table appeared below the ground surface during the period of rainfall, which may lead to landslides. The relationship between precipitation and other factors was established to assess and predict the occurrence of rainfall-induced landslides (Borga et al., 2002; Rosso et al., 2006; Baum et al., 2010). Previous studies have used three main methods to relate precipitation and landslide events: 1. critical rainfall threshold, 2. statistically based landslide susceptibility model, and 3. physically based landslide model (Apip et al., 2010). The rainfall dataset is needed for input in all methods.

The rainfall dataset is generally provided by rain gauges as point measurements. Rain gauges provide accurate rainfall measurements on the ground. However, these are not a true representation of the amount of rain in large areas (Collischonn et al., 2008; García-Pintado et al., 2009). They represent only the small area around the rain-gauge station (Jia et al., 2011). Various factors can cause errors in rain-gauge measurements such as wind, evaporation from the containers, and instrument errors (Ciach, 2003; Cheema & Bastiaanssen, 2012). Villarini et al. (2008) studied the spatial sampling error of rain-gauge measurements and found that the rain-gauge measurement is reasonable for a dense network. If the network is sparse, it becomes necessary to consider spatial sampling uncertainties in the estimation. Because it is difficult to install rain gauges in mountainous areas, it becomes harder to predict and assess landslides in landslide-prone areas. In the last three decades, satellite precipitation measurement projects based on remote sensing techniques such as Tropical Rainfall Measurement

Mission (TRMM) (1997–2014) and Global Precipitation Measurement (GPM) (2014–present) have been developed. Satellite precipitation measurement products have been generated and released to the public. These include the PERSIAN Cloud Classification System, TRMM multi-satellite precipitation analysis (TMPA), and Integrated Multi-satellitE Retrievals for GPM (IMERG) (Prakash et al., 2016, Tang et al., 2016, Chen et al., 2020). Satellite-based rainfall datasets have the advantage of providing full spatial coverage of the areas of interest. However, their spatial resolution is coarse (0.1°× 0.1° grid cell) for the catchment scale analysis (Jia et al., 2011; Cheema & Bastiaanssen, 2012; Huffman et al., 2017; Maidment et al., 2017). Numerous studies attempted to combine the gauge- and satellite-based rainfall productions as an alternative method for water-related disasters, such as floods and landslides (Apip et al. 2010; Immerzeel, 2010; Rossi et al., 2017; Tam et al., 2019). Therefore, the purpose of this study is to develop a framework for a shallow landslide assessment system using satellite rainfall production and a physically based distributed hydrological and geotechnical modelling system.

## 2. FRAMEWORK OF THE RAINFALL-INDUCED LANDSLIDE MODELING SYSTEM

Figure 1 presents the conceptual framework for a physical model of assessing rainfall-induced shallow landslides. Three major parts necessary for developing the rainfall-induced shallow landslide model are discussed: (1) bias correction and spatial downscaling of satellite precipitation; (2) sloping surface infiltration and groundwater table calculation; and (3) calculation of factor of safety based on the infinite slope stability model. The framework of modelling shallow landslides triggered by rainfall was developed on the geographic information system platform. To validate the performance of our framework, the receiver operating characteristic (ROC) curve was selected to test the performance.

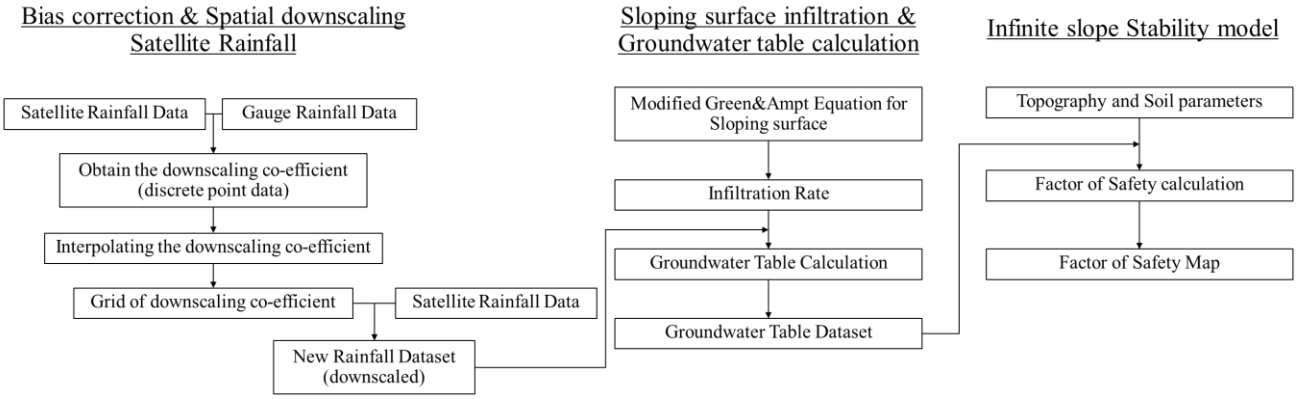


Figure 1. Concept framework of a physical model for assessing rainfall-induced shallow landslides.

### 2.1 Satellite rainfall dataset, bias correction and spatial downscaling method

Satellite rainfall data were obtained from the Integrated Multi-satellitE Retrievals for GPM (IMERG). GPM is a joint project created by the National Aeronautics and Space Administration (NASA), the Japan Aerospace Exploration Agency (JAXA), the Centre National d'Études Spatiales (CNES), the Indian Space Research Organization (ISRO), the National Oceanic and Atmospheric Administration (NOAA), the European Organization for the Exploitation of Meteorological Satellites (EUMETSAT), and others (Huffman et al., 2018). This study uses the IMERG "Final" run V06 which has a 0.1 × 0.1 degree resolution (~10 × 10 km.) and daily interval. The IMERG final run is a satellite product ~3.5 months after the observation month. For gauging rainfall data, our study uses data provided by the Japan Meteorological Agency. A total of 151 rain gauges covering the island of Kyushu of Japan were used to calibrate and downscale the satellite rainfall data.

The downscaling technique in our study is based on the work of Cheema and Bastiaanssen, 2012; Sarr et al., 2015; and Mahmud et al., 2018. First, the ratio of measurement for each rain gauge and the IMERG satellite rainfall was calculated using Eq. (1) to find the downscaling co-efficient. The downscaling co-efficient generated a spatially interpolated map using an inverse distance weighted (IDW) interpolation with 30-meter resolution. Next, the IMERG satellite rainfall was re-gridded from the original resolution to a resolution of 30 meters. Finally, the values from the spatially interpolated map of downscaling co-efficient were multiplied by the values from the re-gridded IMERG satellite rainfall to get the adjusted rainfall dataset.

$$k_{(x,y)} = R_{rain-gauge\,(x,y)} \,/\, R_{sat\,(x,y)} \tag{1}$$

$$R_{adjust\,(x,y)} = R_{sat\,(x,y)} \times k_{(x,y)} \tag{2}$$

where $k_{(x,y)}$ is the downscaling co-efficient at a given point. $R_{rain\text{-}gauges(x,y)}$ is the rain-gauge rainfall data. $R_{sat(x,y)}$ is the satellite rainfall data. $R_{adjust(x,y)}$ is the adjusted rainfall data.

Nash-Sutcliffe efficiency (NSE) and root-mean-square error (RMSE) were used to indicate the performance of before and after in the satellite rainfall dataset. Of all the rain gauges on the island of Kyushu of Japan 85% (128

gauges) were exposed to bias correction and downscaling between the IMERG satellite rainfall dataset and the rain gauges dataset. The remaining 15% (23 rain gauges) were used to validate this procedure. The NSE and RMSE were computed for two measurement pairs: gauge rainfall data versus before-adjusted satellite rainfall data, and gauge rainfall data versus after-adjusted satellite rainfall data. Nash and Sutcliffe (1970) proposed a method to calculate the efficiency index for hydrological models. The NSE presents an index of agreement and disagreement between the observed and computed values whose plot of observed and computed values fits the 1:1 line (Nash & Sutcliffe, 1970; McCuen et al., 2006; Cheema & Bastiaanssen, 2012). The NSE is shown in Eq. (3).

$$NSE = 1 - \left( \sum_{i=1}^{n} \left( R_{rain-gauge(x,y)} - R_{satellite-data(x,y)} \right)^2 / \sum_{i=1}^{n} \left( R_{rain-gauge(x,y)} - \bar{R}_{rain-gauge(x,y)} \right)^2 \right) \quad (3)$$

where $R_{satellite\text{-}data(x,y)}$ is the before and after adjusted satellite rainfall data. $\bar{R}_{rain-gauge(x,y)}$ is the mean rain gauge rainfall data. The range of the NSE value is between -∞ and 1. NSE equal to 1 is the perfect fit for the observed and estimated value (optimal value). NSE equal to 0 means that the data are as accurate as the mean observed value. NSE between 0.0 and 1.0 is commonly viewed as acceptable. (Cheema & Bastiaanssen, 2012; Krakauer et al., 2013).

The RMSE was shown in Eq. (4). The perfect value of the RMSE is 0.

$$RMSE = \sqrt{\left[ \frac{1}{n} \sum_{i=1}^{n} \left( R_{rain-gauge(x,y)} - R_{satellite-data(x,y)} \right)^2 \right]} \quad (4)$$

2.2 Sloping surface infiltration and groundwater table calculation

Infiltration of precipitation is the main supply source of groundwater (Sangrey et al, 1984; Duan et al., 2019). The Green-Ampt infiltration model is widely used to simulate the process of rainfall infiltration into the soil. Chen and Young (2006) modified the Green-Ampt infiltration model for sloping surfaces. The infiltration rate is shown in Eq. (5) and the cumulative infiltration is shown in Eq. (6).

$$i = k_{sat} \left[ \cos\beta + \frac{(\psi \times \Delta\theta)}{I} \right] \quad (5)$$

$$I = (k_{sat} \times t) + \frac{(\psi \times \Delta\theta)}{\cos\beta} \ln\left[ 1 + \frac{I \times \cos\beta}{(\psi \times \Delta\theta)} \right] \quad (6)$$

where $i$ is the infiltration rate. $I$ is the cumulative infiltration. $k_{sat}$ is the saturated hydraulic conductivity of the soil. $\beta$ is the slope angle. $\psi$ is the suction at the wetting front. $\Delta\theta$ is the deficit of the volumetric moisture content.

Based on Darcy's law, Rosso et al. (2006) proposed a groundwater index that is the ratio between the depth of the groundwater table and the depth of the soil, and can be expressed as follows:

$$\omega = h / z \quad (7)$$

where,

$$\omega = \frac{P}{P^*} \left[ 1 - \exp\left( -\frac{1}{A_1} \xi \right) \right], \ \frac{P}{P^*} \le 1 \quad (8)$$

and, for $\frac{p}{p^*} > 1$,

$$\omega = \begin{cases} 1, & \text{if } \xi > -A_1 \ln\left( 1 - \frac{P^*}{P} \right) \\ \frac{p}{p^*} \left[ 1 - \exp\left( -\frac{1}{A_1} \xi \right) \right], & \text{if } \xi \le -A_1 \ln\left( 1 - \frac{P^*}{P} \right) \end{cases} \quad (9)$$

with,

$$p^* = \frac{Tb \sin\beta}{a} \quad (10)$$

with,

$$A_1 = \frac{e}{1+e} \times (1 - S_r) \quad (11)$$

with,

$$\xi = \left( \frac{p^*}{z} \right) t \tag{12}$$

Where $\omega$ is the groundwater table index, $h$ is the depth of the groundwater table, $z$ is the depth of soil, $P$ is the net rainfall as our study refers to the infiltration rate, $T$ is the hydraulic transmissivity, $b$ is the width of channel flow, $a$ is the upslope contributing area, $S_r$ is the degree of saturation, $e$ is the void ratio, and $t$ is rainfall duration.

### 2.3 Infinite slope stability model

During the rainfall period, rainwater seeps into the sloping surface and generates groundwater. This process may lead to slope failure. A shallow landslide has small depth-to-length ratios and failure planes parallel to the slope surface (Zhang et al., 2011). Hence, the infinite slope stability model is widely used to simulate a shallow landside triggered by rainfall. The stability index of the slope is presented as a factor of safety. If the factor of safety is less than 1, the slope is unstable. The factor of safety is the ratio between the shear strength of the slope and the shear stress of the slope. The infinite slope stability equation is shown in Eq. (13).

$$Fs = \frac{c' + \left[ \left( h \times \gamma_{sat} \right) + \left( z - h \right) \gamma_t - \left( h \times \gamma_w \right) \right] \cos^2 \beta \tan \phi'}{\left[ \left( h \times \gamma_{sat} \right) + \left( z - h \right) \gamma_t \right] \sin \beta \cos \beta} \tag{13}$$

where $Fs$ is the factor of safety. $\gamma_{sat}$ is the saturated unit weight of soil. $c'$ is the soil cohesion, $\phi'$ is the friction angle. $\gamma_w$ is the unit weight of water.

## 3. STUDY AREA AND DATASET

### 3.1 Study area

The study area is the small watershed located in the city of Asakura, Fukuoka prefecture, Japan, on the island of Kyushu. This area was affected by tropical storm Nanmadol (2017) which triggered a flood and landslide. Nanmadol (2017) made landfall on Kyushu on 4 July 2017. Figure 2 shows the track of tropical storm Nanmadol (2017), the study area, and the landslide scars. The rainfall during tropical storm Nanmadol (2017) recorded at the Asakura rain gauge station indicated a maximum rainfall of 516 mm. Figure 3 shows the amount of rainfall during tropical storm Nanmadol (2017) when it hit the island of Kyushu. The landslide in Asakura occurred on 5 July 2017.

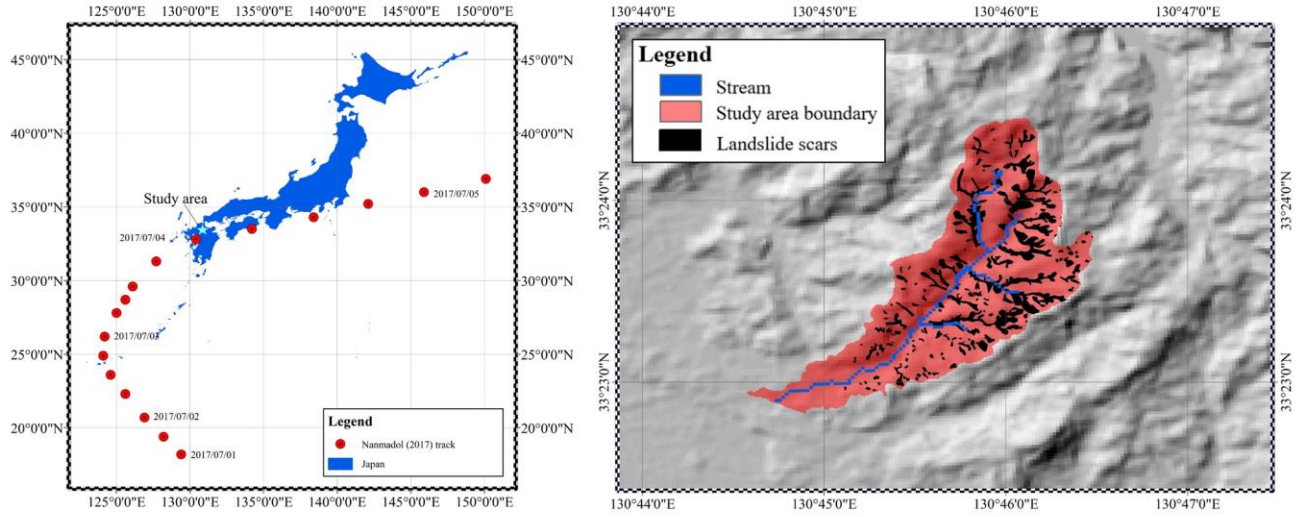


a. b.

Figure 2. a. track of tropical storm Nanmadol (2017), b. study area and landslide scars.

### 3.2 Dataset

After the tropical storm passed over Kyushu, our team investigated affected areas in Asakura. Soil and intact rock samples were collected to determine their engineering properties. According to laboratory testing, the cohesion of the soil was 8 kPa, and the friction angle of the soil was 24.6 degrees. For a spatial map of the basic properties of the soil and depth of the soil layer, our study used global gridded soil information provided by the International Soil Reference Information Centre (ISRIC) (Hengl et al., 2017). Figure 4 shows a map of the soil properties and depth of the soil layer. For a digital elevation model, we used ASTER GDEM V3 developed by the Ministry of Economy, Trade, and Industry (METI) of Japan and the United States National Aeronautics and Space Administration (NASA).

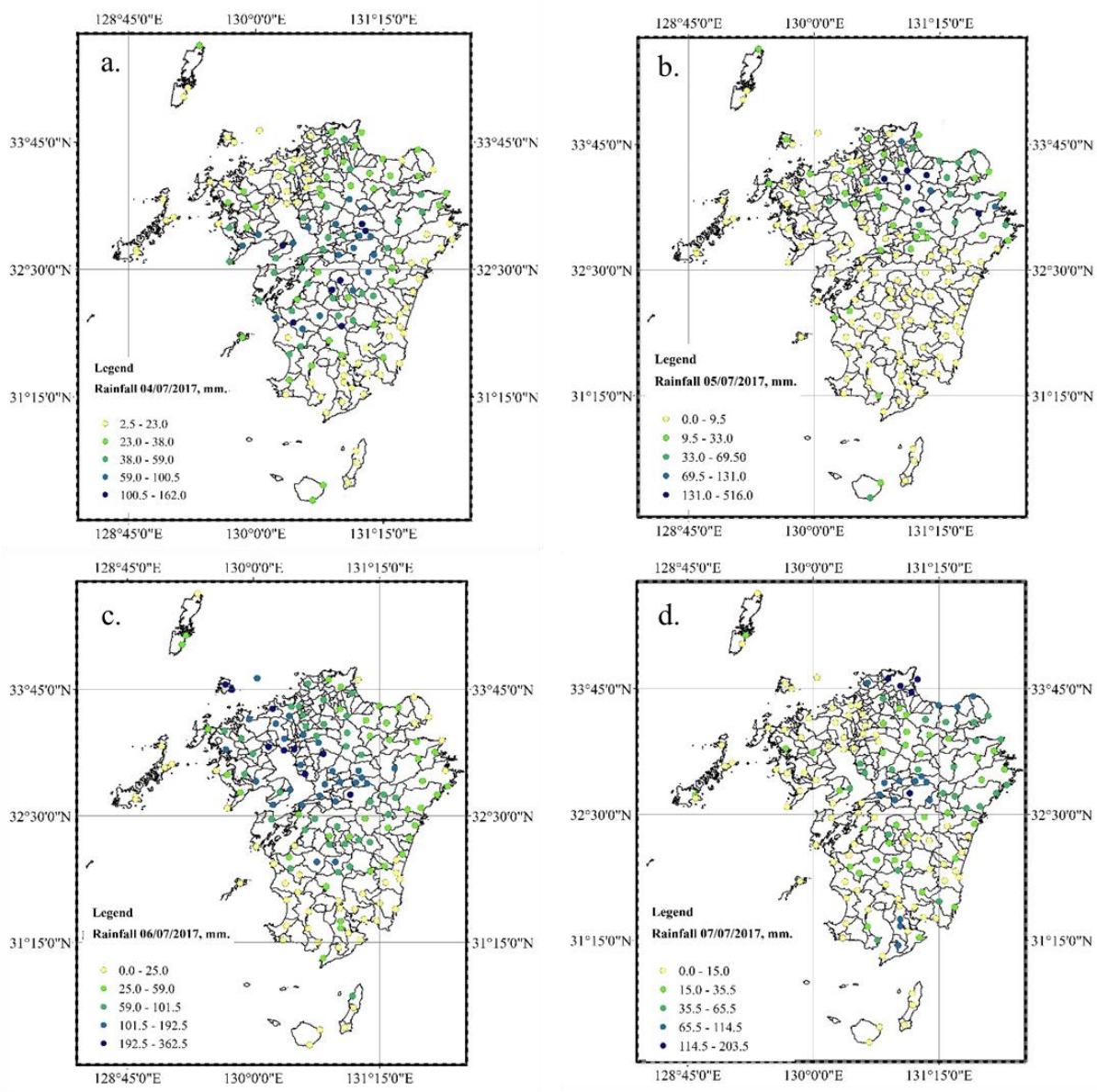


Figure 3. Amount of rainfall during the Tropical storm Nanmadal (2017) hit the island of Kyushu.

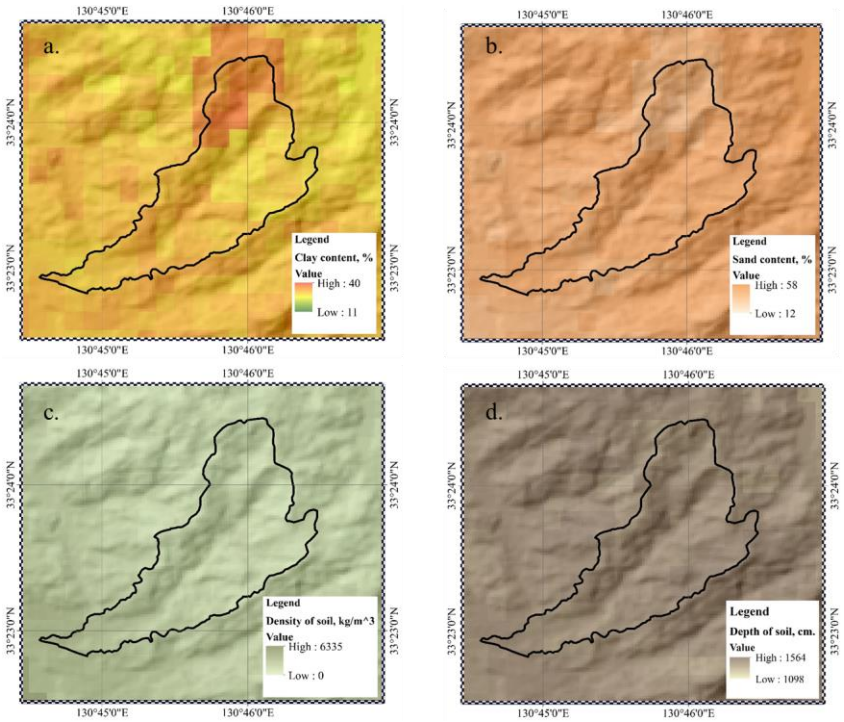


Figure 4. a. clay content, b. sand content, c. density of soil, and d. depth of soil layer.

## 4. RESULTS AND DISCUSSION

Figure 5 shows the daily time series comparison of the gauge rainfall data and the IMERG final run satellite rainfall data. The curve shows that the IMERG final run satellite rainfall data both overestimated and underestimated the gauge rainfall data. Jiang and Bauer-Gottwein (2019) mentioned that the correlation of IMERG satellite rainfall data and gauge rainfall data increases with longer time scales. Based on their research, the daily scale was the lowest correlation compared with the monthly and yearly scales. Considering the scatter plot of IMERG satellite rainfall and gauge rainfall before correction, the satellite rainfall almost underestimated the gauge rainfall when the amount of gauge rainfall was higher than 100 mm. When gauge rainfall measured 0 to 100 mm, the IMERG final run satellite rainfall both overestimated and underestimated the gauge rainfall. The RMSE of uncorrected satellite rainfall was approximately 47.15 mm. The NSE value of uncorrected satellite rainfall was approximately 0.045. After bias correction, the graph clearly shows that the satellite rainfall data improved. The RMSE of corrected satellite rainfall is approximately 43.02 mm and the NSE value is approximately 0.205.

Figure 6 is a spatial map of uncorrected/corrected satellite rainfall data and gauge rainfall data from 4 July 2017 through 7 July 2017. When comparing the rainfall distribution patterns of uncorrected satellite rainfall and gauge rainfall, we found that the uncorrected satellite rainfall and gauge rainfall had similar distribution patterns. The IMERG satellite rainfall data could show areas with high-intensity rainfall. However, the magnitude of the IMERG satellite rainfall data was different from the gauge rainfall data. After downscaling and bias correction, the distribution and magnitude of adjusted rainfall data were fairly similar to the gauge rainfall data.

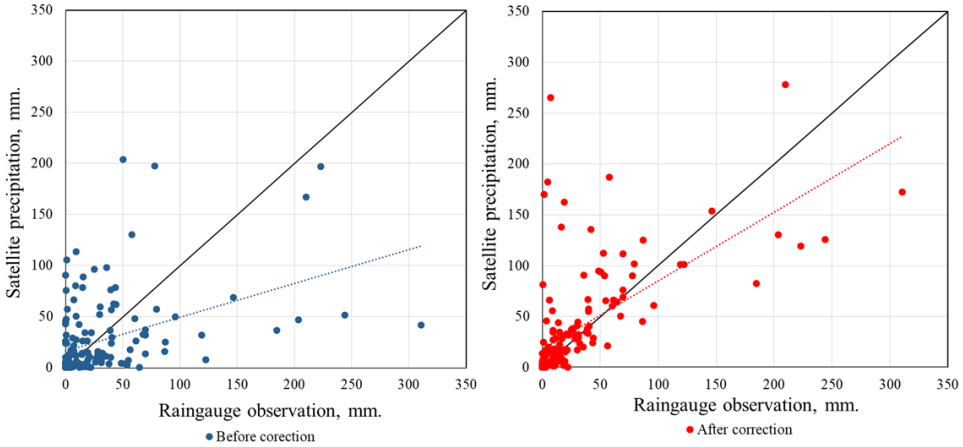


Figure 5. Scatter plot showing the relationship between gauge rainfall data and the IMERG final run satellite rainfall data.

Our proposed framework was performance tested by using the event of a shallow landslide triggered by tropical storm Nanmadol (2017) in Asakura. Figure 7 shows the safety factor map on 05 July 2017. We used the receiver operating characteristic (ROC) curve to evaluate the performance of our proposed framework. The ROC curve compares our simulated results with the actual landslide. The red areas unstable areas simulated by the proposed framework, and the factor of safety in those areas is less than 1. The simulated stable areas have a factor of safety of more than 1. The black labels indicate the actual shallow landslide scars. According to our calculations, the true positive rate was 0.48 and the false positive rate was 0.12. The accuracy of the proposed framework for a physical model of assessing rainfall-induced shallow landslides using satellite rainfall data was 0.8. The area under curve (AUC) of ROC was 0.67. This is quite low. However, the accuracy of the proposed framework is satisfactory. Since the true positive rate value is quite low, the predicted unstable areas do not quite match the actual landslide scars. The false-positive rate is low, which is a good result meaning that the predicted stable areas are well matched with the actual stable areas. Overall, in our performance summary, the ROC curve of the proposed framework is above the random line. This means that the performance of our proposed framework is acceptable and moderately good. Figure 8 shows the receiver operating characteristic curve of our study.

The maps of the factor of safety and the actual landslide areas show that the shallow landslide occurred on the steep slope and valley. The landslide areas occurred on high upslope contributing area values. The locations and densities of landslide occurrences are related to the conditions of the upslope contributing area and slope (Yamashita et al., 2017).

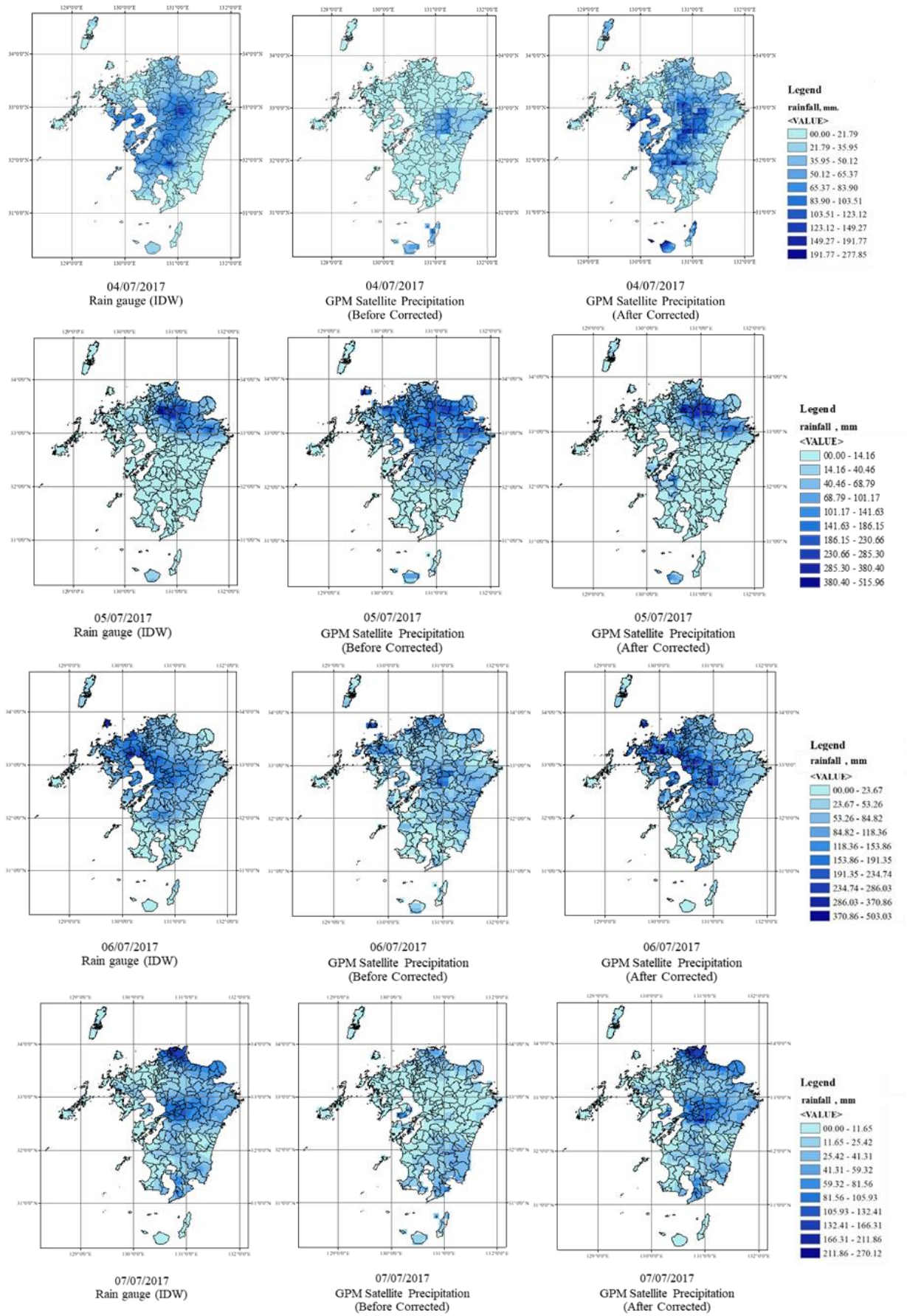


Figure 6. Spatial map of uncorrected/corrected satellite rainfall data and gauge rainfall data.

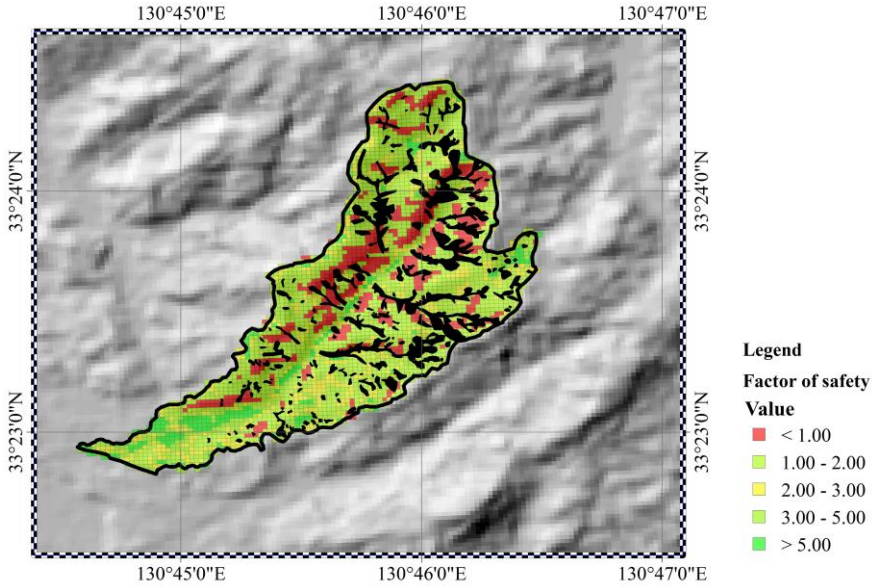


Figure 7. The factor of safety map on 05 July 2017.

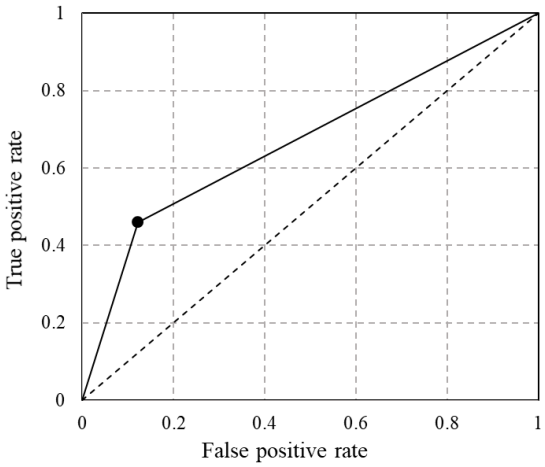


Figure 8. Receiver operating characteristic curve of the study.

## 5. CONCLUSIONS

The IMERG final run satellite rainfall can illustrate the distribution of rainfall. The magnitude of the IMERG final run satellite rainfall both underestimates and overestimates; thus, it should be calibrated with the gauge rainfall values. According to our evaluation of the performance of the framework for a physical model of assessing rainfall-induced shallow landslides, the accuracy is 0.8 and the area under curve of ROC is 0.67. Therefore, the application of corrected satellite rainfall is a good alternative to simulate rainfall-induced shallow landslides. This study demonstrated that the proposed framework has the potential to become a practical method for assessing shallow landslide hazards on a regional scale. However, downscaling and bias correction must be further developed and improved to increase the performance of the model. Also, the spatial distribution of the shear strength parameters, cohesion of soil, and friction angle are a significant challenge in calculating the factor of safety map.

## ACKNOWLEDGMENTS

The authors are grateful to the Japan Meteorological Agency (JMA) for the gauge rainfall data and the Geospatial Information Authority of Japan (GSI) for the aerial photography of the disaster areas. Thankfully acknowledged is the Land Processes Distributed Active Archive Center (LP DAAC) and NASA's Earth Science Data Systems Program for digital elevation model datasets. Finally, the authors would like to thank the Precipitation Measurement Missions of the United States National Aeronautics and Space Administration (NASA) for the IMERG satellite rainfall data.

## REFERENCES

Apip, Takara, K., Yamashiki, Y., Sassa, K., Ibrahim, A. B., and Fukuoka, H. (2010). A distribution hydrological-geotechnical model using satellite-derived rainfall estimates for shallow landslide prediction system at a catchment scale. *Landslides*, 7:237-258.

Baum, R. L., Godt, J. W., and Savage W. Z. (2010). Estimating the timing and location of shallow rainfall-induced landslide using a model for transient, unsaturated infiltration. *JOURNAL OF GEOPHYSICAL RESEARCH*, 115:1-26.
Borga, M., Fontana, G. D., Gregoretti, C., and Marchi, L. (2002). Assessment of shallow landsliding by using a physically based model of hillslope stability. *HYDROLOGICAL PROCESSES*, 16:2833-2851.
Chaithong, T., Komori, D., Sukegawa Y., Touge, Y., Mitobe, Y., and Anzai, S. (2018). Landslides and precipitation characteristic during the Typhoon Lionrock in Iwate prefecture, Japan. *International Journal of Geomate*, 14(44):109-114.
Cheema, M. J. M., and Bastiaanssen, W. G. M. (2012). Local calibration of remotely sensed rainfall from the TRMM satellite for different period and spatial scales in the Indus Basin. *International Journal of Remote Sensing*, 33(8): 2603-2627.
Chen, H., Yong, B., Shen, Y., Liu J., Hong, Y., and Zhang, J. (2020). Comparison analysis of six purely satellite-derived global precipitation estimates. *Journal of Hydrology*, 581:1-14.
Ciah, G. J. (2003). Local random errors in Tipping-Bucket rain gauge measurements. *Journal of atmospheric and oceanic technology*, 20:752-759.
Collischonn, B., Collischonn, W., and Tucci, C. E. M. (2008). Daily hydrological modeling in the Amazon basin using TRMM rainfall estimates. *Journal of Hydrology*, 360:207-216.
Duan, G., Chen, D., and Niu, R. (2019). Forecasting groundwater level for soil landslide based on a dynamic model and landslide evolution pattern. *Water*, 11:1-13.
Garcı´a-Pintado, J., Barbera´ G. G., Erena M., and Castillo V. M. (2009). Rainfall estimation by rain gauge-radar combination: a concurrent mulitlicative-additive approach. *WATER RESOURCES RESEARCH*, 45:1:15.
Hazarika, H., Yamamoto, S., Ishizawa, T., Danjo, T., Kochi, Y., Fujishiro, T., Okamoto, K., Matsumoto, D., and Ishibashi, S. (2020). The 2017 July Northern Kyushu torrential rainfall disaster-geotechnical and geological perspectives. *Chapter 1 in Developments in Geotechnical Engineering: Geotechnics for Natural Disaster Mitigation and Management*, 1-19.
Hengl, T., Jesus, J. M. D., Heuvelink, G. B. M., Gonzalez, M, R., Kilibarada, M., Blagotic, A., Shangguan, W., Wright, M. N., Geng, X., Bauer-Marschallinger, B., Guevara, M. A., Vargas, R., Macmillan, R. A., Batjes, N. H., Leenaars, J. G. B., Ribeiro, E., Wheeler, I., Mantel, S., Kempen, B. (2017). SoilGrids250m: Global gridded soil information based on machine learning. *PLOS ONE*, 1-40.
Huffman, G. J., Bolvin, D. T., and Nelkin, E. J. (2017). Integrated multi-satellite retrievals for GPM (IMERG) technical documentation. *IMERG Tech Document*.
Huffman, G., Bolvin, D. T., Braithwaite, D., Hsu, K., Joyce, R., Kidd, C., Nelkin, E. J., Sorooshian, S., Tan, J., and Xie, P. (2018). Algorithm theoretical basis document (ATBD) version 5.2, *NASA Global Precipitation Measurement (GPM) integrated Multi-satellitE Retrievals for GPM (IMERG)*, 1-35.
Immerzeel, W. W. (2010). Bias correction for satellite precipitation estimation used by the MRC Mekong flood forecasting system. *Mission report – Mekong river commission*, 1-32.
Jia, S., Zhu, W., Lu, A., and Yan, T. (2011). A statistical spatial downscaling algorithm of TRMM precipitation based on NDVI and DEM in the Qaidam basin of China. *Remote Sensing of Environment*, 115:3069-3079.
Jiang, L. and Bauer-Gottwein, P. (2019). How do GPM IMERG precipitation estimates perform as hydrological model forcing? Evaluation for 300 catchment across mainland China. *Journal of Hydrology*, 572:486-500.
Krakauer, N. Y., Pradhanang, S. M., Lakhankar, T., and Jha, A. K. (2013). Evaluating satellite products for precipitation estimation in mountain regions: a case study for Nepal. *Remote sensing*, 5(8):4107-4123.
Kawamoto, K., Oda M., and Suzuki, K. (2000). Hydro-Geological study of landslides caused by heavy rainfall on August 1998 in Fukushima, Japan. *Journal of Natural Disaster Science*, 22:13-23.
Lim, T. T., Rahardjo, H., Chang, M. F., and Fredlund, D. G. (1996). Effect to rainfall on matric suction in a residual soil slope. *Can. Geotech. J*, 33:618-628.
Macuen, R. H., Knight, Z., and Cutter, A. G. (2006). Evaluation of the Nash-Sutcliffe efficiency index. *Journal of Hydrologic Engineering*, 11(6):597-602.
Maidment, R. I., Grimes, D., Black, E., Tarnvsky, E., Young, M., Greatrex, H., Allan, R. P., Stein, T., Nkonde E., Senkunda, S. and Alcantara, E. M. U. (2017). A new, long-term daily satellite-based rainfall dataset for operational monitoring in Africa. *Scientific data*, 4(170063):1-17.
Murakami, Y., Shimizu, O., Sato, S., and Yamada, T. (2008) Sediment-related disaster caused by Typhoon 0310 (Etau) in Hidaka region of Hokkaido, Japan. *International Journal of Erosion Control Engineering*, 1:30-37.
Nash, J. E., and Sutcliffe, J. V. (1970). River flow forecasting through conceptual models part I – a discussion of principles. *Journal of Hydrology*, 10:282-290.
Prakash, S., Mitra, A., Pai, D. S., and Aghakouchak, A. (2016). From TRMM to GPM: how well can heavy rainfall be detected from space?. *Advances in Water Resources*, 88:1-7.
Rossi, M., Krischbaum, D., Valigi D., Mondini A. C. and Guzzetti, F. (2017). Comparison of satellite rainfall estimates and rain gauge measurements in Italy, and impact on landslide modeling. *Climate*, 5(90):1-30.
Rosso, R., Rulli, M. C., and Vannucchi, G. (2006). A physically based model for the hydrologic control on shallow landsliding. *WATER RESOURCSE RESEARCH*, 42:1-16.
Sakurai, M. (2014). Landslide disaster of Izu-Oshima Island by Typhoon No. 26 in 2013. *J. of the Jpn. Landslide Soc.*, 51(1):25-28.
Sangrey, D. A., Harrop-Williams, K. O., Klaiber, J. A. (1984). Predicting ground-water response to precipitation. *Journal of Geotechnical Engineering*, 110(7):957-975.
Sarr, M. A., Seidou, O., Tramblay, Y., and Adlouni, S. E. (2015). Comparison of downscaling methods for mean and extreme precipitation in Senegal. *Journal of Hydrology: Reginal Studies*, 4:369-385.

Sehara, Y., Suzuki M., Yamamoto T., Terayama T., Tomokiyo T., and Kochi, Y. (2006). Slope disasters caused by Typhoon No. 14 of 2005 in Yamaguchi prefecture. *Soils and Foundations*, 46(6):817-830.

Tang, G., Wen Y., Zheng Y., Long, D., and Hong, Y. (2016). From Tropical to Global precipitation measurement initial validation and application (Chapter 1), *Hydrologic Remote Sensing capacity building for sustainability and resilience*, pp. 3-15.

Taniguchi, Y. (2008). Sediment disasters caused by Typhoon No. 14, 2005, in Miyazaki prefecture. *International Journal of Erosion Control Engineering*, 1:11-19.

Tam, T. H., Rahman, M. Z. A., Harun, S., Hanapi, M. N., and Kaoje, I. U. (2019). Application of satellite rainfall products for flood inundation modelling in Kelantan river basin, Malaysia. *Hydrology*, 6(95):1-20.

Yamashita, K., Hattanji, T., Tanaka, Y., Doshida, S., and Matsushima, T. (2017). Topographic characteristics of rainfall-induced shallow landslides on granitic hillslopes: a case study in Hofu city, Yamaguchi prefecture, Japan. *Tsukuba Geoenvironmental Sciences*, 13:23-29.

Yokoyama, S., Murai, M., Nakaya S., Nishiyama, K., Ohaka, K., and Nakano, H. (2006). Fractured zone landslide and debris flow at Azue, Naka town, Tokushima prefecture, induced by the heavy rainfall of Typhoon Namtheum in 2004. *Jour. Geol. Soc. Japan*, 112:137-151. (In Japanese)

Villarini, G., Mandapaka, P., Krajewski, W. F., and Moore, R. J. (2008). Rainfall and sampling uncertainties: a rain gauge perspective. *Journal of Geophysical Research*, 113:1-12.